Journal of Solid State Chemistry 195 (2012) 161–165

Contents lists available at SciVerse ScienceDirect

Journal of Solid State Chemistry

journal homepage: www.elsevier.com/locate/jssc

$Na_2Ge_2Se_5$: A highly nonlinear optical material

In Chung [a], Jung-Hwan Song [b,†], Joon I. Jang [b,1], Arthur J. Freeman [b], Mercouri G. Kanatzidis [a,*]

[a] Department of Chemistry, Northwestern University, Evanston, IL 60208, USA
[b] Department of Physics and Astronomy, Northwestern University, Evanston, IL 60208, USA

ARTICLE INFO

Available online 5 June 2012

Keywords:
Nonlinear optics
Chalcogenides
Second harmonic generation
Semiconductors
Layered compounds
Density functional calculations

ABSTRACT

We report an integrated experimental and theoretical study of the two-dimensional polar selenogermanate compound $Na_2Ge_2Se_5$, which exhibits strong nonlinear optical (NLO) second harmonic generation response in the visible and infrared region. The compound is type-I phase-matchable with a large SHG coefficient $\chi^{(2)} \approx 290$ pm V^{-1}, which is the second highest among the phase-matchable NLO materials. It also performs as an NLO frequency mixer to produce radiation via difference frequency generation. The compound is optically transparent from the visible (0.521 μm) to the far IR (18.2 μm) and melts congruently. *Ab initio* density functional theory band structure calculations show that the unusually large second-order optical nonlinearity is attributed to the two-dimensional character of the crystal structure. Raman, IR and optical absorption spectroscopy, differential thermal analysis, NLO properties of derivatives of $Na_2Ge_2Se_{4.55}Te_{0.45}$ and $Na_2Ge_{1.64}Sn_{0.36}Se_5$ and thermal expansion behavior studies are also reported.

1. Introduction

Commercially viable lasing sources with reasonable wavelength range and efficiency are still limited despite the development of tunable laser technology over the past two decades [1]. Second–order nonlinear optical (NLO) phenomena are highly desirable because they allow new coherent light sources of different frequencies with the potential for tunability. For example, three-wave mixing is an effective way of producing coherent light at frequencies where lasers perform poorly or are unavailable. Two light waves ω_1 and ω_2 interact with each other as well as with an NLO medium, generally inorganic crystals, generating a third wave: four different new frequencies of $2\omega_1$ and $2\omega_2$ by second harmonic generation (SHG) and mixed frequencies $|\omega_1 \pm \omega_2|$ by difference and sum frequency generation (DFG and SFG) [2].

There have been multiple NLO applications, for example, affordable blue lasing sources, parametric generation of tunable lights, all-optical photonic and high-capacity communication networks and optical storages [3]. Many of these have included oxides such as $LiNbO_3$ and $KTiOPO_4$ [4].

Currently, particular interest focuses on infrared light sources that are widely tunable and coherent in the spectral region of 2–12 μm. This is the finger-print region for organic and inorganic molecules. Accordingly, it is critical for sensing illicit and hazardous materials such as chemical warfare agents, [5] biohazards, [6] explosives, [7] pollutants and trace gas [8] for homeland security, environmental monitoring and industrial process controls. Tunable, narrow band lasers are also necessary for minimal invasive medical surgery [9] and direct imaging of anisotropic biological structures in tissues, cell metabolism and disease states such as Alzheimer's disease and cancer [10,11].

Oxide NLO materials are unsuitable for IR applications due to their critical IR absorptions. Practical use of organic/polymer NLO materials is significantly restricted by poor thermal stability and high IR absorption, despite their high optical nonlinearity [12].

Currently, IR NLO materials with excellent performance are relatively rare and have limited structural diversity. Benchmark materials are mostly three-dimensional chalcopyrite compounds such as $ZnGeP_2$ ($\chi^{(2)}$=150 pm/V) and AMQ_2 (A=Ag, Li; M=Ga, In; Q=S, Se, Te); [4] and zincblende compounds such as GaAs ($\chi^{(2)}$=181.6 pm/V) and GaP ($\chi^{(2)}$=95.3 pm/V) [2]. The former adopt a uniaxial, diamond-like structure due to a slight distortion from the isotropic cubic zincblende structure and have moderate performance. The latter exhibit high second-order nonlinearity and mid-IR transparency, however, they are optically isotropic and, as a result, non-birefringent and non-phase-matchable [2].

Recently, we reported the $APSe_6$ (A=K, Rb), [13–15] $A_2P_2Se_6$ (A=K, Rb, Cs) [16] and $AZrPQ_6$ (Q=S, Se), [17] $k_2Hg_3Sn_2S_8$ [17b] which are phase-matchable and exhibit large SHG coefficients: $APSe_6$, $\chi^{(2)} \approx 150$ pm/V; $K_2P_2Se_6$, $\chi^{(2)} \approx 53.7$ pm/V [14,16,18]. They are widely transparent in the IR region and melt congruently. Our first

* Corresponding author. Fax: +1847 491 5937.
E-mail address: m-kanatzidis@northwestern.edu (M.G. Kanatzidis).
† Deceased.
[1] Current address: Department of Physics, Applied Physics and Astronomy, State University of New York at Binghamton, NY 13902, USA.

0022-4596/$ - see front matter © 2012 Elsevier Inc. All rights reserved.
http://dx.doi.org/10.1016/j.jssc.2012.05.038

principles electronic band structure calculations on those materials showed that the low-dimensionality of the structure with large covalency in the atomic bonds are the origin of such large SHG coefficients [18]. We also demonstrated that the $APSe_6$ can be processed into amorphous and crystalline fibers and thin films with strong and permanent SHG and DFG responses [13,14].

Here we report the new infrared–visible NLO material $Na_2Ge_2Se_5$ and its derivatives, $Na_2Ge_2Se_{4.55}Te_{0.45}$ and $Na_2Ge_{1.64}Sn_{0.36}Se_5$ [19]. $Na_2Ge_2Se_5$ melts congruently and is widely transparent from the visible (0.52 μm) to far IR (18.2 μm) spectral region. It outperforms most phase-matchable NLO inorganic materials with the exceptional SHG coefficient $\chi^{(2)}=287.5\pm3.2$ pm/V, except for $CdGeAs_2$ (434 pm/V). The observed value is remarkable considering its wide optical band gap of 2.38 eV, compared to other top IR NLO materials: GaSe ($\chi^{(2)}=108\pm22$ pm/V, $E_g=2.0$ eV),[4] $ZnGeP_2$ ($\chi^{(2)}=150$ pm/V, $E_g=2.0$ eV), $AgGaTe_2$ ($\chi^{(2)}=102$ pm/V, $E_g=1.36$ eV) and $AgGaSe_2$ ($\chi^{(2)}=66$ pm/V, $E_g=1.83$ eV) [20]. Generally, NLO compounds with a smaller band gap exhibit larger $\chi^{(2)}$ but result in a narrower transparency window and a lower damage threshold [21]. For example, the usefulness of $CdGeAs_2$ is severely restricted by its very small band gap of 0.57 eV. Only few lasers can operate $CdGeAs_2$ with the typical need of cryogenic temperature. *Ab initio* density functional theory calculations on $Na_2Ge_2Se_5$ using the full potential linearized augmented plane wave (FLAPW) method [22] show its unusually large SHG coefficient is derived from the two-dimensional crystal structure of the compound.

$Na_2Ge_2Se_5$ crystallizes in the polar space group of $Pna2_1$ [23,24]. It features a layered anionic framework of $^2_\infty[Ge_2Se_5^{2-}]$ separated by Na^+ ions (Fig. 1a). The polar structure arises from both the $^2_\infty[Ge_2Se_5^{2-}]$ anionic layer and arrangement of Na^+ cations. The main building block of the anionic layer is a $[GeSe(\mu_2\text{-}Se_{3/2})]$ tetrahedron. These tetrahedra condense via two shared corners to form a helical chain running down the *c* axis, which is the polar axis of the $Pna2_1$ space group (Fig. 1b). These helical strands align parallel with identical handedness and link to adjacent chains to form the $^2_\infty[Ge_2Se_5^{2-}]$ layers via corner-sharing Se atoms (Fig. 1c). There exist two such layers in the unit cell and they are related by a 2_1 screw axis running along the *c*-direction. From a different point of view, the layers consist of fused $[Ge_6Se_6]$ rings (Fig. 1c).

There are two crystallographically unique Ge atoms. The Ge–Se distances are normal; those to bridging Se atoms range from 2.3686(9) to 2.3957(9) Å and those to terminal Se atoms are shorter from 2.275(1) to 2.282(1) Å. The $[GeSe_4]$ tetrahedra are distorted; the angles of Se–Ge–Se bonds range from 97.88(3) to 116.09(4)° for the Ge(1) atom and from 99.66(3) to 118.53(4)° for the Ge(2) atom.

Of the two crystallographically distinct Na atoms, Na(1) adopts a regular octahedral geometry with six Se atoms and Na(2) is in a normal pentagonal bipyramidal configuration with seven Se atoms. The $[Na(1)Se_6]$ and $[Na(2)Se_7]$ polyhedra condense via edge-sharing to form a helical chain parallel to the polar *c* axis. The chains aligned with the same handedness connect via corner sharing to form the infinite $^2_\infty[Na_2Se_5^{8-}]$ sheet (Fig. 2).

The noncentrosymmetric crystal structure of $Na_2Ge_2Se_5$ is unique among the relevant members of $A_2M_2Q_5$ and $A_4M_4Q_{10}$ (A=alkali metal; M=Si, Ge, Sn; Q=S, Se) family. Those with smaller atoms preferably adopt discrete adamantine-like $[M_4Q_{10}]^{4-}$ cluster anions and crystallize in the centrosymmetric space group *Cmcm*, as shown in $Na_4Si_4Q_{10}$ and $Na_4Ge_4S_{10}$. Some with bigger congeners form a layered structure but also crystallize in a centrosymmetric space group, for example, $Na_2Sn_2Se_5$ (*Pbca*) and $K_2Sn_2Q_5$ (Q=S, Se; *C2/c*). $Na_2Ge_2Se_5$ allows only limited ability to accommodate Sn and Te atoms into its structure. The maximum fractions we were able to achieve and still isolate pure isostructural phases were $Na_2Ge_{1.64}Sn_{0.36}Se_5$ and $Na_2Ge_2Se_{4.55}Te_{0.45}$.

According to differential thermal analysis (DTA) at a rate of 10 °C/min, $Na_2Ge_2Se_5$ melts at 576 °C and crystallizes at 509 °C upon cooling (Supporting Information Figure S2). The X-ray powder diffraction patterns before and after melting/recrystallization were identical. The results indicate congruent melting of the compound. The thermal expansion of $Na_2Ge_2Se_5$ was determined by X-ray single crystal diffraction study in the range of 300–500 K (Figure S3). The linear (Eq. (1)) and volumetric thermal expansions (Eq. (2)) are defined as

$$\alpha_t = \frac{1}{L_t}\frac{dL_t}{dT} \quad (1)$$

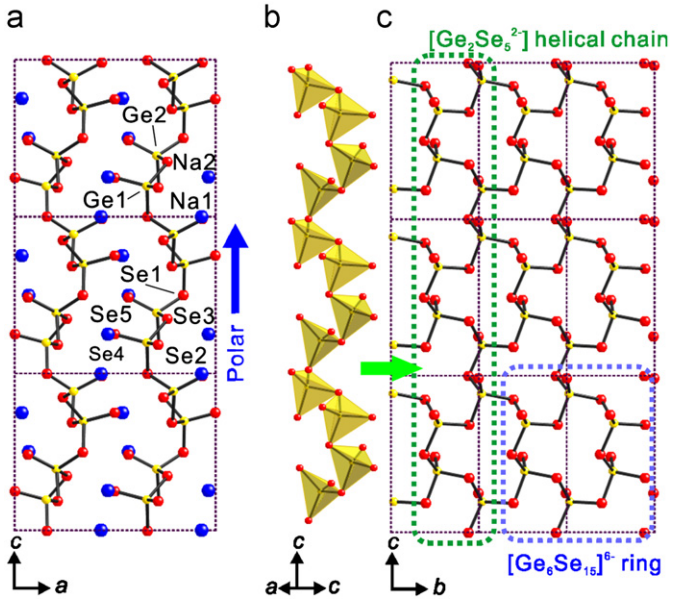

Fig. 1. (a) Structure of $Na_2Ge_2Se_5$ viewed down the *b* axis, (b) a single strand of the $^1_\infty[Ge_2Se_5^{2-}]$ helical chain running along the *c* axis (the polar axis of the $Pna2_1$ space group) in a polyhedral presentation and (c) segment of the $^2_\infty[Ge_2Se_5^{2-}]$ sheet viewed down the *a* axis. Na blue, Sn yellow, Se red. (For interpretation of the references to color in this figure legend, the reader is referred to the web version of this article.)

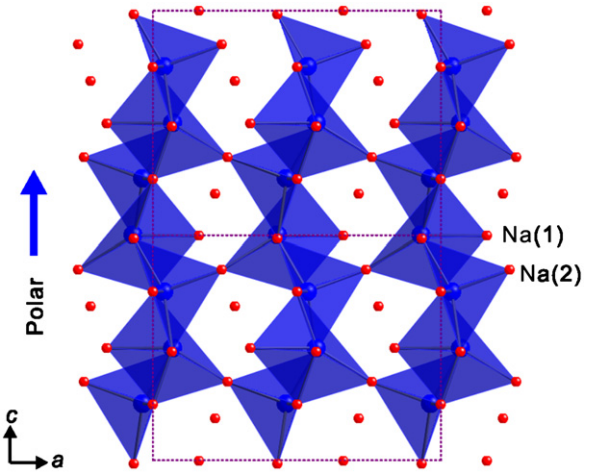

Fig. 2. Organization of Na^+ ions in the structure of $Na_2Ge_2Se_5$. The $^2_\infty[Na_2Se_5^{8-}]$ layer viewed down the *b* axis. The Na–Se distances are from 2.887(3) to 3.341(4) Å with longer Na(1)–Se(2) distances of 3.664(4) Å and Na(2)–Se(2) of 3.687(4) Å. Na blue, Se red. (For interpretation of the references to color in this figure legend, the reader is referred to the web version of this article.)